Computational modeling of cracking of concrete in strong discontinuity settings

J. Oliver†, A. Huespe‡, M.D.G. Pulido‡† and S. Blanco‡‡

ETS Enginyers de Camins, Canals i Ports de Barcelona, Technical University of Catalonia (UPC), Campus Nord UPC, Edifici C-1, C/Jordi Girona 1-3, 08034 Barcelona, Spain

(Received June 27, 2003, Accepted September 15, 2003)

Abstract. The paper is devoted to present the Continuum Strong Discontinuity Approach (CSDA) and to examine its capabilities for modeling cracking of concrete. After introducing the main ingredients of the CSDA, an isotropic continuum damage model, which distinguishes tension and compression states, is used to implicitly induce a projected traction separation-law that rules the cracking phenomena. Criteria for onset and propagation of material failure and specific finite elements with embedded discontinuities are also briefly sketched. Finally, some representative numerical simulations of cracking, in plain and reinforced concrete specimens, using the CSDA are presented.

Keywords: concrete; crack modeling; strong discontinuity; continuum damage.

1. Introduction: crack modeling in concrete

Inelastic behavior of concrete structures is intimately related to crack formation. In a first stage microcrack nucleation and growing can be observed in the so-called fracture process zone. After that, in a second stage micro cracks coalesce and macrocracks, which propagate throughout the body, are visible.

In the first stage, the number of microcracks is large and densely distributed, which makes suitable the continuum model hypothesis for the analysis. Phenomenological continuum damage models, see for example Lemaitre (1985), have been introduced in the past as a way of describing the nucleation and growth of microcracks. They make use of the effective stress concept, initially introduced by Kachanov (1958). Strain softening and elastic stiffness degradation are fundamental characteristics of these models.

However, it is well known that constitutive models equipped with strain softening fail to describe the solid fracture process since the resulting boundary value problem becomes ill posed. Numerous procedures have been presented in the past to circumvent this deficiency as, for instance, non-local modes, gradient models, rate dependent models, etc.

In recent years the so-called strong discontinuity approach (SDA) has became a promising

† Professor
‡ Researcher from CIMEC-Conicet-UNL, Argentina
‡† Assitant Professor
‡‡ Researcher Assistant

methodology to analyze failure in concrete structures caused by crack propagation. Detailed descriptions can be found, for instance, in Simo, *et al.* (1993), Oliver (1996), Armero, *et al*. (1996), Larsson, *et al.* (1996), Borja (2000), Wells, *et al*. (2001). As a specific branch of the SDA, the continuum strong discontinuity approach (CSDA) emphasizes the use of continuum formats to model displacement discontinuities (see Oliver, *et al*. (1999), Oliver (2000), Oliver, *et al*. (2002) for a complete description). In there, it is proved that, with appropriate ingredients, any standard continuum (stress-strain) constitutive model projects onto the discontinuity interface, in form of a traction-separation model typical of cohesive discrete fracture mechanics. Therefore, that projection introduces a natural way of modeling fracture and cracking processes in concrete by means of continuum constitutive models. The procedure bridges fracture and damage mechanics, since the same continuum model describes both the degradation into the fracture process zone and, after material instability onsets, the discrete traction-separation law governing the macro-fracture propagation.

In this work, after a description of the continuum strong discontinuity approach and the corresponding numerical simulation procedures, that methodology is used to model development of cracking in several problems in order to make an assessment of both the viability and potentiality of the CSDA for modeling cracking in concrete.

2. The continuum strong discontinuity approach (CSDA)

The CSDA grounds on classical continuum mechanics by generalizing the admissible displacement space, i.e. : the occurrence of fractures in the solid medium is captured by introducing discontinuous displacement fields in the problem. The resulting kinematics, termed strong discontinuity kinematics, requires a reinterpretation of the constitutive model to make it capable of dealing with the unbounded strains emerging from those discontinuous displacement fields. In fact, from equilibrium requirements, the constitutive model should furnish bounded stresses even for unbounded strains. This can be achieved through the redefinition of only one parameter: the softening modulus, which has to be regularized in points where unbounded strains take place. The rest of ingredients and features of the continuum constitutive model remain unmodified.

The corresponding numerical procedures should preserve that characteristic kinematics by allowing capturing discontinuous displacement fields. The so-called finite elements with embedded discontinuities fulfill this condition, and therefore, they become a fundamental ingredient of the approach.

The strong discontinuity kinematics, the adapted continuum constitutive model and the use of specific discontinuous finite elements, are then the fundamental aspects of the CSDA that are described in this Section.

2.1. Strong discontinuity kinematics

An admissible displacement field $\mathbf{u}(\mathbf{x})$ exhibiting displacement discontinuities can be described by (see Fig. 1):

$$\mathbf{u}(\mathbf{x}) = \bar{\mathbf{u}}(\mathbf{x}) + \mathcal{H}_S[[\mathbf{u}]](\mathbf{x}) \; ; \quad \mathcal{H}_S = \begin{cases} = 1 \forall \mathbf{x} \in \Omega^+ \\ = 0 \forall \mathbf{x} \in \Omega^- \end{cases} \tag{1}$$

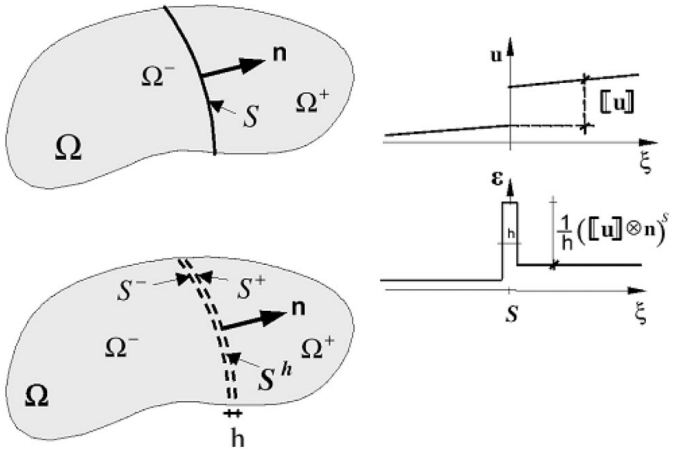

Fig. 1 Strong discontinuity kinematics

where $\bar{\mathbf{u}}$ is a smooth field and $\mathcal{H}_S[[\mathbf{u}]](\mathbf{x})$ ($\mathcal{H}_S$ being the Heaviside/step function shifted to S) captures the displacement jump field $[[\mathbf{u}]](\mathbf{x})$ at the discontinuity interface S of normal $\mathbf{n}$, which divides the body Ω into two disjoints parts Ω^+ and Ω^-. The strain field kinematically compatible with the discontinuous displacement field (1) is then:

$$\boldsymbol{\varepsilon}(\mathbf{x}) = \nabla^S \mathbf{u}(\mathbf{x}) = \underbrace{\bar{\boldsymbol{\varepsilon}}(\mathbf{x})}_{\substack{\text{regular}\\ \text{(bounded)}}} + \underbrace{\delta_S([[\mathbf{u}]] \otimes \mathbf{n})^{\text{sym}}}_{\substack{\text{singular}\\ \text{(unbounded)}}}, \tag{2}$$

which displays un unbounded term due to the presence of the Dirac's delta function δ_S.

For computational purposes, the singular term in Eq. (2) should be regularized through the following "h-sequence", in terms of the bandwidth h, of the regularization domain S^h (see Fig. 1):

$$\delta_S(\mathbf{x}) = \lim_{h \to 0} \frac{\mu_S}{h} \; ; \; \mu_S(\mathbf{x}) = \begin{cases} = 1 \forall \mathbf{x} \in S^h \\ = 0 \;\; \text{otherwise} \end{cases} \tag{3}$$

2.2. Isotropic continuum damage model for concrete

Although the CSDA is not restricted to any specific constitutive model, let us consider an isotropic continuum damage model which belongs to the family of classical continuum damage models (see for example Lemaitre (1985)) where a scalar internal variable $d \in [0, 1]$ describes the elastic stiffness degradation (d=0 for the undamaged material and d=1 for the fully damaged material). According to Oliver (2000) the damage variable d is made dependent on an internal strain-like variable r. The model can then be described as follows:

Free energy: $$\varphi(\boldsymbol{\varepsilon}, r) = (1-d)\varphi_o \; ; \; \varphi_o = \frac{1}{2}\boldsymbol{\varepsilon} : \mathbf{C} : \boldsymbol{\varepsilon} \tag{4}$$

Damage variable: $$d(r) = 1 - \frac{q(r)}{r}; \tag{5}$$

Internal variable: $$\dot{r} = \lambda \; ; \; r|_{t=0} = r_o = \sigma_u / \sqrt{E} \tag{6}$$

Constitutive equation $$\boldsymbol{\sigma} = (1-d)\mathbf{C}:\boldsymbol{\varepsilon} = \frac{q}{r}\underbrace{\mathbf{C}:\boldsymbol{\varepsilon}}_{\bar{\boldsymbol{\sigma}}} = \frac{q}{r}\bar{\boldsymbol{\sigma}} \tag{7}$$

Damage function $$\begin{aligned} & g(\boldsymbol{\varepsilon}, r) \equiv \tau_\varepsilon(\boldsymbol{\varepsilon}) - r \\ & \tau_\varepsilon(\boldsymbol{\varepsilon}) \equiv \sqrt{\bar{\boldsymbol{\sigma}}^+ \cdot \mathbf{C}^{-1} \cdot \bar{\boldsymbol{\sigma}}} \end{aligned} \tag{8}$$

Loading conditions: $$\lambda \geq 0 \; ; \; g \leq 0 \; ; \; \lambda g = 0 \tag{9}$$

Softening law: $$\dot{q} = H\dot{r} \; ; \; H(r) = \begin{cases} H_0 = \text{constant} \rightarrow (\text{linear softening}) \\ H_0 \exp\left(\frac{-r_0}{G_f}(r - r_o)\right) \rightarrow (\text{exponent softening}) \end{cases} \tag{10}$$

Incremental constitutive law: $$\dot{\boldsymbol{\sigma}} = \mathbf{C}^{\tan}:\dot{\boldsymbol{\varepsilon}} \; ; \; \mathbf{C}^{\tan} = \begin{cases} \mathbf{C}^{unl} \equiv (1-d)\mathbf{C} = \frac{q}{r}\mathbf{C} \qquad (\text{unloading}) \\ \mathbf{C}^{load} \equiv \frac{q}{r}\mathbf{C} - \frac{q - Hr}{r^3}\bar{\boldsymbol{\sigma}} \otimes \bar{\boldsymbol{\sigma}}^+ \; (\text{loading}) \end{cases} \tag{11}$$

where $\varphi(\boldsymbol{\varepsilon}, r)$ is the free energy, depending on the strain tensor $\boldsymbol{\varepsilon}$ and the internal variable r, and φ_o is the elastic strain energy for the undamaged material; $\mathbf{C} = \bar{\lambda}(\mathbf{1} \otimes \mathbf{1}) + 2\mu\mathbf{I}$ is the elastic constitutive tensor, $\bar{\lambda}$ and μ are the Lame's parameters and $\mathbf{1}$ and $\mathbf{I}$ are the identity tensors of 2nd and 4th order respectively.

In Eq. (7), : $\bar{\boldsymbol{\sigma}} = \mathbf{C}:\boldsymbol{\varepsilon}$ is the effective stress. Its positive counterpart is then defined as:

$$\bar{\boldsymbol{\sigma}}^+ = \langle \bar{\sigma}_i \rangle \, \mathbf{p}_i \otimes \mathbf{p}_i \tag{12}$$

where $\langle \bar{\sigma}_i \rangle$ stands for the positive part (Mac Auley brackets) of the i-th principal effective stress $\bar{\sigma}_i$ ($\langle \bar{\sigma}_i \rangle = \bar{\sigma}_i$ for $\bar{\sigma}_i \geq 0$ and $\langle \bar{\sigma}_i \rangle = 0$ for $\bar{\sigma}_i < 0$) and $\mathbf{p}_i$ stands for the i-th principal stress eigenvector. The initial elastic domain defined as $E_\sigma^0 := \{\boldsymbol{\sigma}; \sqrt{\boldsymbol{\sigma}^+ \cdot \mathbf{C}^{-1} \cdot \boldsymbol{\sigma}} < r_o\}$ is then unbounded

for compressive stress states $\boldsymbol{\sigma}^{+} = \mathbf{0}$ and, therefore, damage becomes only associated to tensile stress states as usual for modeling cracking in concrete.

The actual stresses $\boldsymbol{\sigma}$ and the stress-like variable q are determined via the state Eqs. (7) and (10). Eq. (10) defines the softening law in terms of the continuum softening parameter $H \leq 0$. In Eq. (6), σ_u and E are, respectively, the tensile strength and the Young's modulus. Finally, Eq. (11) is the rate constitutive law in terms of the tangent constitutive operator $\mathbf{C}^{\tan}$.

2.3. Softening modulus regularization

As the discontinuous displacement field (1) is activated, the unbounded strains in Eq. (2) develop inside S^h. Furthermore, the equilibrium condition imposes the tractions $\boldsymbol{\mathcal{T}} = \boldsymbol{\sigma} \cdot \mathbf{n}$ to be continuous in the neighborhood of S^h. Since the strains and stresses are regular outside S^h that condition enforces boundedness of the traction vector $\boldsymbol{\mathcal{T}} = \boldsymbol{\sigma}_{S^h} \cdot \mathbf{n}$, and therefore of the whole stress tensor, in S^h which, in consequence, has to be bounded in presence of unbounded strains. As it has been proven in Oliver (2000) a sufficient condition for this to happen is to redefine the character of the softening modulus H as follows :

$$\frac{1}{H} = \delta_S \frac{1}{\bar{H}}; \tag{13}$$

where $\bar{H}$ is termed the intrinsic softening modus, and can be characterized as material parameter in terms of the fracture energy G_f the ultimate tensile strength σ_u and the Young's modulus E :

$$\begin{aligned} \bar{H} &= -\frac{\sigma_u^2}{2EG_f} && \text{(linear softening)} \\ \bar{H} &= -\frac{\sigma_u^2}{EG_f} \exp\left(\frac{-r_o}{G_f}(r - r_o)\right) && \text{(exponent softening)} \end{aligned} \tag{14}$$

Eq. (14) clearly links the CSDA with non-linear fracture mechanics via the classical concept of fracture energy. The regularized version of Eq. (14) reads, after insertion of Eq. (3):

$$H = h\bar{H} \tag{15}$$

which is the so called softening regularization condition.

2.4. Induced discrete constitutive model: traction separation law

The introduction, in the continuum constitutive model in Eqs. (4) to (11), of the strong discontinuity kinematics (2)-(3) and the softening modulus regularization (15), leads to a crucial result in the CSDA. In fact, it can be shown, see Oliver (2000), that a discrete constitutive damage model relating the traction $\boldsymbol{\mathcal{T}} = \boldsymbol{\sigma} \cdot \mathbf{n}$ and the displacement jump $[[\mathbf{u}]]$ is automatically fulfilled at the failure (cracking) interface S i.e.:

$$\mathcal{T}=(1-\omega)\,\mathbf{Q}\cdot[[\mathbf{u}]]\ ;\ \mathbf{Q}\ =\ \mathbf{n}\cdot\mathbf{C}\cdot\mathbf{n} \tag{16}$$

were ω is a discrete damage variable having a different character respect to the continuum one (d in Eq. (5)). This model is a projection of the original constitutive model into the failure surface and inherits its properties. Therefore, discrimination from tension to compression in Eq. (12) is implicitly fulfilled in Eq. (16). It is important to emphasize that this discrete constitutive model is neither derived nor implemented in practice, but fulfilled from the aforementioned ingredients, while enjoying the physical significance of the continuum model. This fact constitutes one of the most relevant benefits of the CSDA.

2.5. Local material failure. Cracking propagation direction

Detection of material failure in concrete and, consequently, onset of cracking, is many times established in terms of the maximum principal (tensile) stress as it reaches the uniaxial strength σ_u. The fracture propagation direction is then orthogonal to that principal stress.

Nevertheless, onset of local failure can be determined in a more mechanically rigorous and consistent way, from the material stability properties of the continuum constitutive model. Loss of strong ellipticity of the tangent constitutive operator $\mathbf{C}^{load}$ in Eq. (11) signals the time, t_B, at which bifurcation of the stress-strain field (material instability) takes place. This can be set in terms of the so-called localization tensor $\mathbf{Q}^{\text{loc}}$ as:

$$\begin{aligned}&\det(\mathbf{Q}^{\text{loc}}(\mathbf{x},\mathbf{n},t_B))=\mathbf{0}\\&\mathbf{Q}^{\text{loc}}(\mathbf{x},\mathbf{n},t_B)=\mathbf{n}\cdot\mathbf{C}^{load}\cdot\mathbf{n}\end{aligned} \tag{17}$$

from which the normal $\mathbf{n}$, orthogonal to the propagation direction, can be determined (see for example Runesson, *et al*. (1991) and Oliver, *et al*. (2003b)).

Both criteria can be inserted in the CSDA. The first one provides many times enough accurate results for tensile dominated damage phenomena as cracking. On the other side, the use of the criterion (17) seems relevant when plastic dissipation dominates the failure, like in compression failure in concrete or in metals. In any case, in the context of the CSDA the relevant aspect of detection of local failure is the activation, at the corresponding material point, of the strong discontinuity kinematics (2)-(3), associated to the selected direction $\mathbf{n}$.

3. Numerical aspects. Finite elements with embedded discontinuities

Numerical implementation of the CSDA lies on the so-called finite elements with embedded discontinuities, see Oliver, *et al*. (2003a), admitting discontinuous displacement fields. They consist of adding, to the basic displacement modes, an enriching mode $\mathcal{M}_s(\mathbf{x})[[\mathbf{u}]]^e$, whose shape function $\mathcal{M}_s(\mathbf{x})$ exhibits a unit jump in the element, as shown in Fig. 2. The elemental jump is constant along the elemental discontinuity interface S^e, and the resulting displacement jump field is discontinuous between elements.

The orientation of S^e is provided by the local material failure criterion discussed in the previous sections. Its position inside every element results from specific algorithms devoted to track the

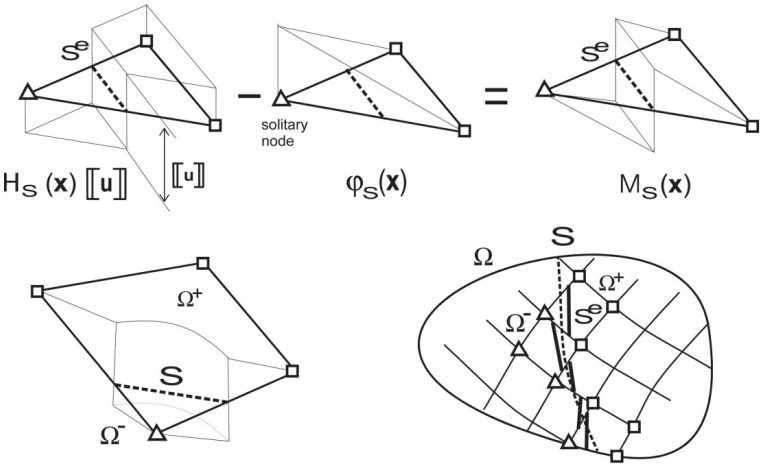

Fig. 2 Elemental enrichment of triangles and quadrilaterals

propagation of every crack. In Oliver, *et al*. (2002) a global tracking algorithm capable to deal with multiple, and simultaneously propagating, cracks is presented.

4. Representative numerical simulations

A series of numerical simulations of fracture and cracking in concrete is presented in this section. One of the aims is to assess the numerical results (both quantitative and qualitative) in front of well-documented experiments. An additional goal is to show the possibilities of the CSDA to capture multiple crack formation mechanisms in reinforced concrete structures.

Several cases of fracture propagation in typical mode I and mixed mode, as categorized by fracture mechanics, are presented. Although there is no consensus about the question if mixed-mode fracture actually exists in heterogeneous materials like concrete, typical examples of those modes are presented. In the first and second simulations, the slip displacement jump is at least one order smaller than the opening mode, this characterizing a mode I of fracture. In the third simulation, both magnitudes are much closer to each other, this approaching a mixed-mode of fracture.

The numerical results have been obtained using the general-purpose finite element code COMET (Cervera, *et al*. 2001) where the specific ingredients of the CSDA have been implemented.

4.1. Notched specimen in Mode I of fracture

The concrete, 0.0508[m] of thickness, specimen of Fig. 3 with a crack line wedge, is analyzed assuming a plane stress state. It is subjected to a wedge couple of loads F_1 and diagonal compression forces F_2 changing along time as shown in Fig. 3(b). Kobayashi, *et al.* (1985) published experimental results of this test. In Rots (1988) a numerical simulation based on the smeared crack approach can be found.

The material model parameters are: Young's modulus E=30.5(GPa), Poisson's ratio ν=0.2, ultimate tensile strength σ_u=3.(MPa) and fracture energy G_f=100.(N/m). The finite element mesh consists of 1332 enhanced linear triangles.

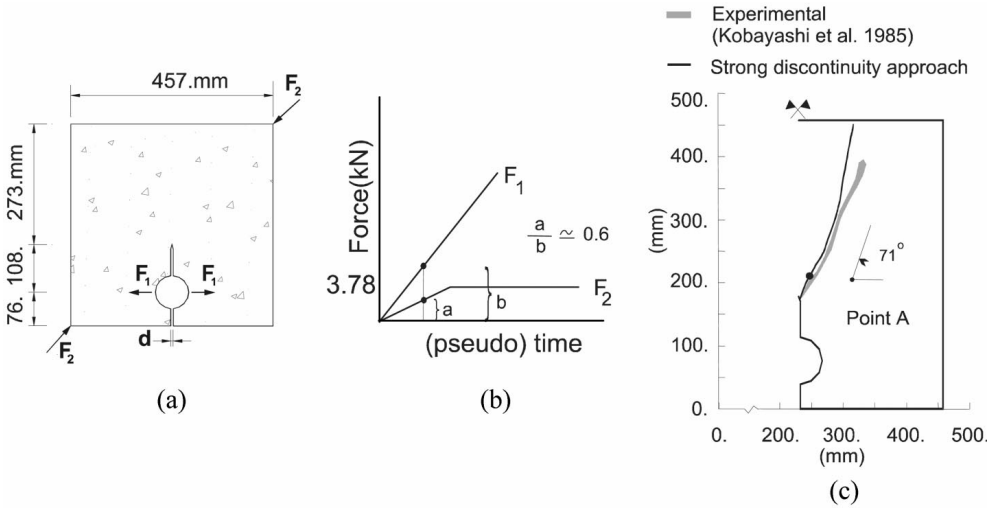

Fig. 3 Concrete fine slab specimen fracturing in mode I

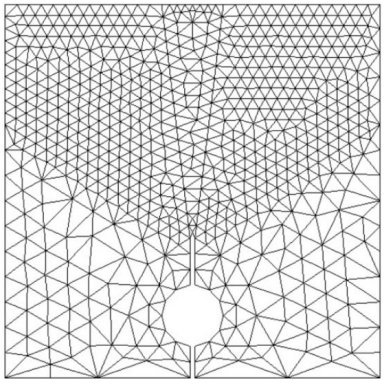

Fig. 4 Concrete fine slab specimen fracturing in mode I. Finite element mesh: 1332 enhanced linear triangles, 2048 nodes

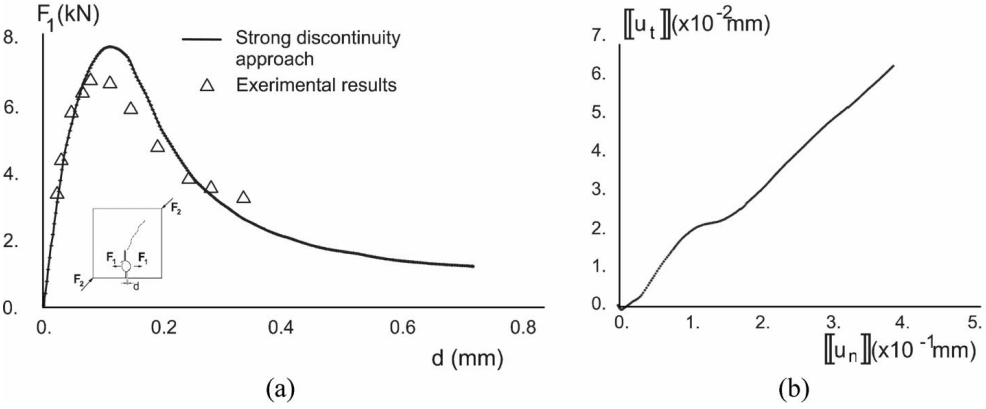

Fig. 5 Concrete fine slab specimen. Load vs. displacement curves

The fracture propagates in mode I from the notch toward the upper part of the specimen displaying an approximately constant angle of 71^o with the horizontal axis. In Fig. 3(c) the numerically obtained fracture path is compared with the experimental one.

Fig. 5(a) shows the load vs. CMOD curve. There it can be checked a slight limit load overestimation and a good agreement in the post-critical stage. Fig. 5(b) stresses the mode I character of the obtained numerical results by displaying the normal versus tangential jump displacement at point A of Fig. 3(c).

4.2. Concrete L-shaped panel

L-shaped concrete specimens are popular benchmark tests for validation of computational models. The one considered here, performed by Winkler, Niederwanger and Hofstetter is fully described in NW-Ialad (2003). A schematic diagram is represented in Fig. 6.

The material parameters are the following: E=25859.(MPa), σ_u=2.70(MPa), ν=0.2. The fracture energy value G_f=90.5(N/m) was obtained by integrating the experimental curve load-vertical displacement at the load application point (see Fig. 7) and dividing this value by the total length of the crack shown in Fig. 6.

A potential-type softening law was considered. The evolution of the continuum softening parameter H in Eq. (11) is given by $H(q)=\alpha q^{\beta}$ where the material parameters α and β are:

$$\alpha = -\left(\frac{\sigma_u}{\sqrt{E}}\right)^{(2-\beta)} \frac{1}{(2-\beta)G_f} \; ; \; \beta = 1.5$$

The fracture problem has been modeled by six different meshes:

- 1071, 3007 and 6645 triangles (meshes 1, 2 and 3 respectively) and
- 627, 1555 and 3401 quadrilaterals (meshes 4, 5 and 6).

Numerically obtained load versus δ_v curves are plotted in Fig. 8 and Fig. 9 and compared with the experimental results.

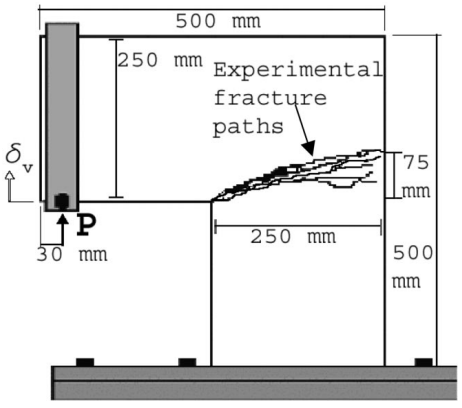

Fig. 6 Concrete *L*-shaped panel. Experimental fracture paths

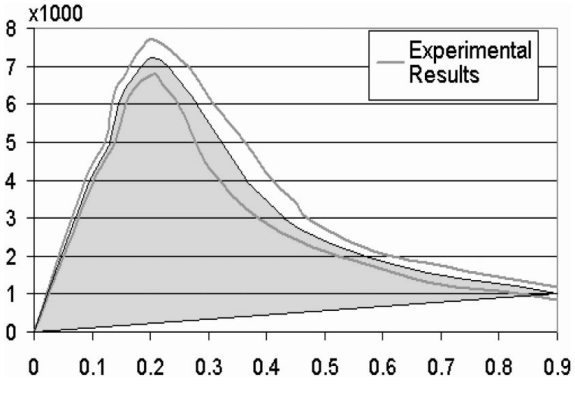

Fig. 7 Experimental force P[N] vs. displacement δ_v[mm] curve and determination of the fracture energy

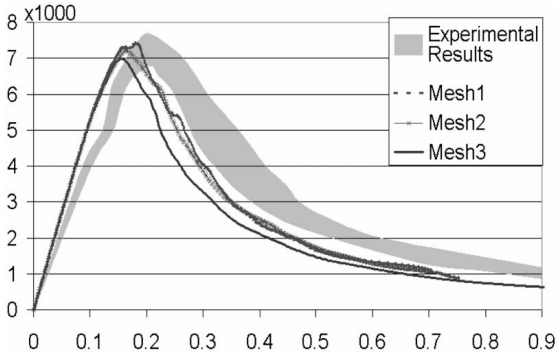

Fig. 8 P[N] vs. δ_v [mm] curves. Triangular meshes

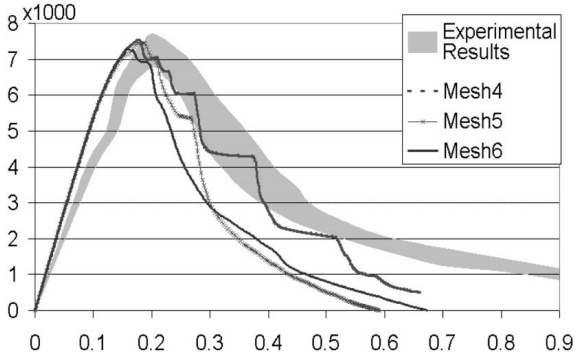

Fig. 9 P[N] vs. δ_v [mm] curves. Quadrilateral meshes

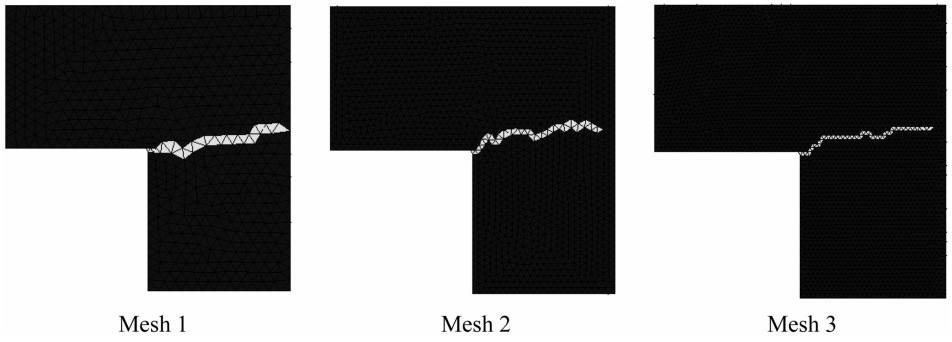

Fig. 10 Crack paths (triangular meshes)

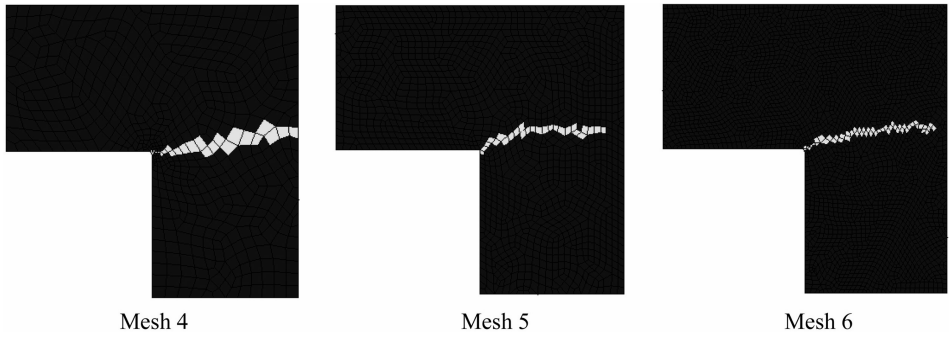

Fig. 11 Crack paths (quadrilateral meshes)

In Figs. 10 and 11 the numerically obtained crack paths, for these meshes, are displayed. It is remarkable that, in spite of the different type and number of elements, the results are very similar in all the cases.

4.3. Double notched specimen in mixed mode of fracture

A double-notched concrete specimen undergoing a mixed mode fracture is analyzed. Nooru-Mohamed (1992) has presented experimental results of this test. Nechnech (2001) and Spencer (2002) reported numerical solutions.

The specimen is a concrete block, of 200×200 [mm] size and 50.[mm] of thickness, with two depth symmetrical notches as shown in Fig. 12(a). It is fixed to the loading device on those sides where loading and displacement conditions are imposed. An initial horizontal load force $P_h = 5.(kN)$ is applied, which remains constant through the complete experiment. In a second stage, the loading device imposes an incremental vertical displacement δ_v. Plane stress assumption has been taken for the modeling. Material parameter values are: E=30.[Gpa], ν=0.2, σ_u=3.(MPa). In the spirit of the CSDA the fracture energy G_f=110.(N/m) has been considered the same for both fracture modes I and II.

The finite element mesh has 1572 quadrilateral elements including the rigid support, which has

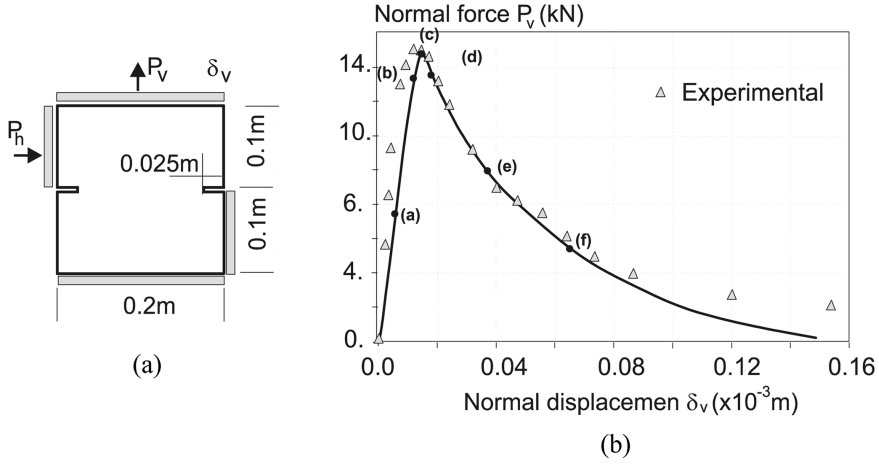

Fig. 12 Double-notched concrete specimen: (a) schematic diagram of the experimental test; (b) vertical force versus vertical displacement curve. Experimental results from Nooru-Mohamed (1992), taken from Nechnech (2001)

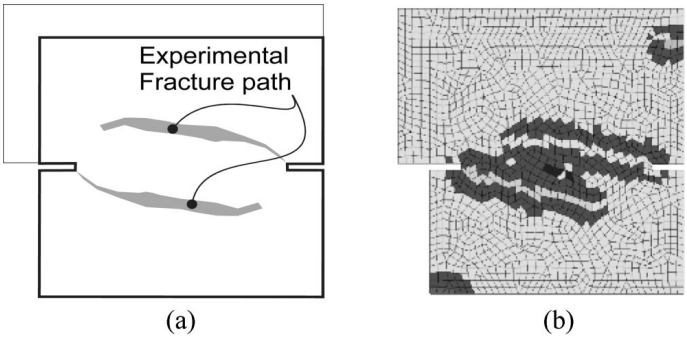

Fig. 13 Double-notched concrete specimen: (a) experimental crack pattern (taken from Spencer, 2002); (b) numerical crack pattern

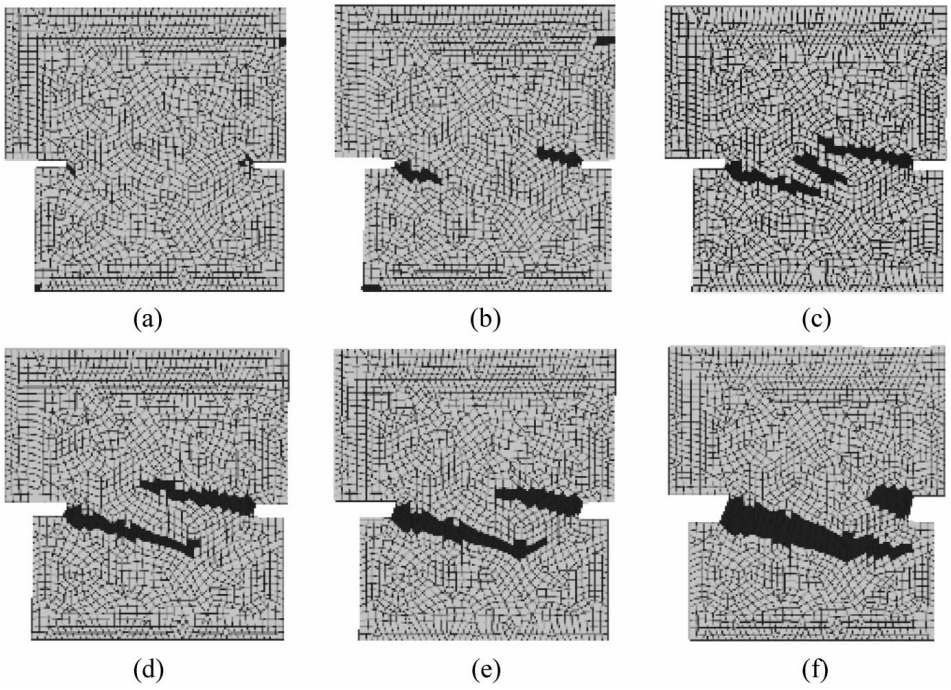

Fig. 14 Double-notched concrete specimen: crack pattern evolution at different stages marked at the load-displacement curve in Fig. 12

also been modeled.

Fig. 12(b) shows the vertical force versus the vertical displacement both for numerical simulation and the experiment. It can be observed that numerical results provide a slight underestimation of the initial stiffness, but the peak load and the post-peak curve agree very well with the experimental test. In Fig. 13 the numerical obtained crack patterns and the experimental ones display an excellent agreement.

Fig. 12(b) displays in dark gray, elements belonging to a zone surrounding the fracture paths, which are determined by the algorithm tracing the discontinuity line. Those elements are forbidden to get a failure state by imposing an elastic response. This condition provides a more robust numerical response.

Fig. 14 presents the evolution of the crack pattern obtained at different stages of the numerical simulation. In this case, the propagation direction was considered orthogonal to the first tensile principal stress.

4.4. Crack development in a reinforced concrete specimen

The goal of the test is to qualitatively reproduce the sequential process of formation of cracks, at the neighborhood of the reinforcement, due to the bond-slip effects in the concrete/steel interface. It is not intended to make an exhaustive study but to check if the proposed methodology could capture the essentials of cracking generation phenomena.

In the model a reinforced concrete specimen is subjected, under plane strain conditions, to a pull

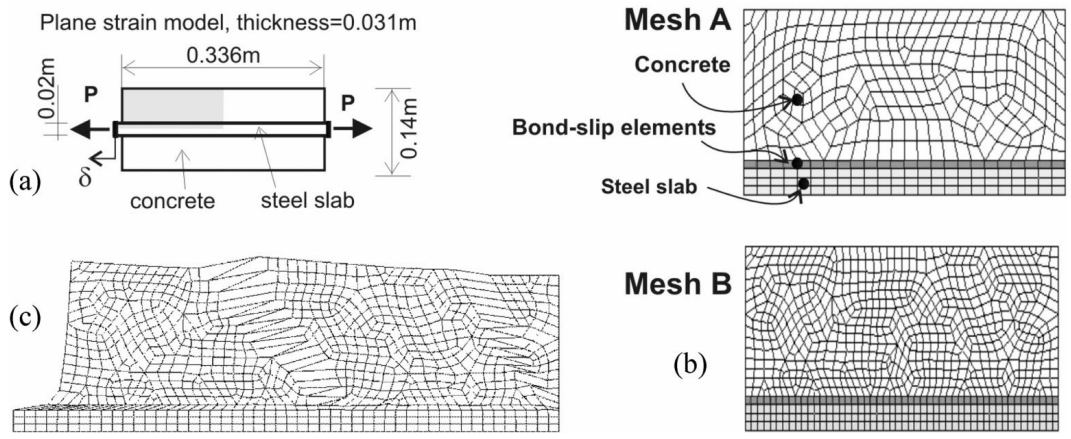

Fig. 15 Reinforced concrete specimen. (a) geometrical model; (b) coarse and fine meshes; (c) deformed mesh after the primary cracks have propagated

Table 1 Material properties

Material	Model	E	ν	G_f	σ_u
Concrete	Only traction damage	25. GPa	0.18	25 N/m	2.8 MPa
Reinforcement	Elastic	214. GPa	0.3	--	--
Joint	Rigid-Plastic (J_2)	----	0.3	--	3.0 MPa

out state in the rebar as shown in Fig. 15(a) (in Rots (1988) a numerical solution of a similar configuration, assuming axial symmetry can be found).

Adhesion along the steel-concrete interface is modeled using bond-slip elements with a rigid-perfectly plastic J_2 material model. Additional material parameters characterizing the problem, Young's modulus, E, Poisson's ratio, ν, ultimate tensile strength, σ_u, and fracture energy, G_f of concrete, as well as steel parameters and the sliding stress, σ_{yd}, of the bounding material are displayed in Table 1.

Due to the problem symmetries, only one fourth of the specimen was discretized. In order to check mesh sensitivity two different finite element meshes, A and B in Fig. 15(b), were considered. Since similar results were obtained, no comparison is presented in terms of the density of the finite element mesh.

Results in Figs. 16 and 17, although not experimentally assessed, display the phenomena observed in reinforced concrete structures i.e.: in a first stage of the loading process development of a

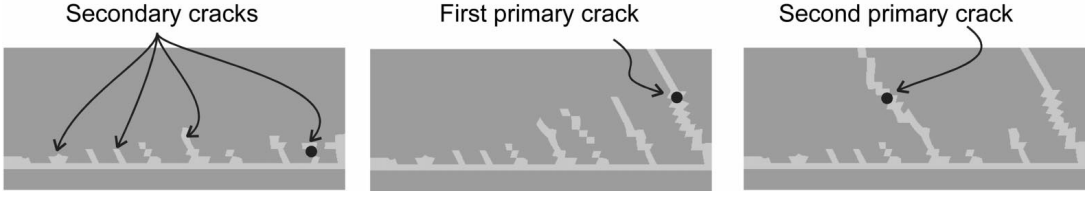

Fig. 16 Reinforced concrete specimen. Crack patterns along the failure evolution process

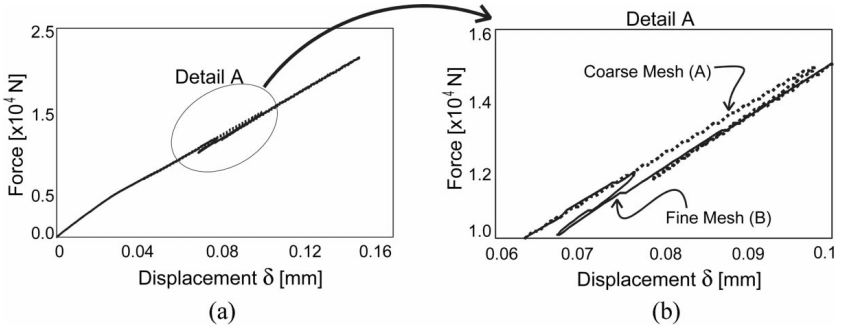

Fig. 17 Reinforced concrete specimen. Equilibrium curve and detail of the snap-back zone

secondary crack system takes place without causing substantial loss of the structural strength. Then, a loading increase leads to the formation of primary crack systems propagating across the concrete section, resulting into a sudden loss of strength of the structure.

This characteristic feature is also present in the numerical solution. The load P vs. displacement δ curve of Fig. 17(a), the detail of this curve in Fig. 17(b) and the crack system developed in the concrete bulk in Fig. 16 show that a severe snap-back behavior is associated with the propagation of a primary crack through the corresponding concrete section. However, after that, the load carrying capacity of the reinforced concrete structure is not yet exhausted since a subsequent reloading translates into the development of a second primary crack in front of the first one. For a longer specimen the process would continue from the center to the end. The crack spacing would then depend on the concrete/steel material and geometrical properties but, essentially, on the adhesion properties of the interface.

5. Concluding remarks

In the preceding sections, the most relevant ingredients of the CSDA have been introduced and the approach has been applied to the numerical modeling of concrete cracking for a representative set of examples. From them, and from the authors' experience in using that approach in modeling additional problems, the following remarks can be made:

- Limit loads provided by the numerical simulations are acceptable. However, in some cases, the numerical response displays a slightly more rigid (or flexible in other cases) pre-peak structural response when compared with experimental results. This fact is also found in the literature by using alternative numerical solution procedures. Since this seems to be a well-fitted part of the simulation, mainly affected by theoretically well-determined material parameters, reasons for those discrepancies could be either the accuracy of the reported experimental results or an intrinsic feature of the considered type of finite element to be determined in subsequent research.
- In the CSDA the softening law and the intrinsic softening parameter $\overline{H}$ in Eq. (14) governs the post-peak response stage. Therefore, the accuracy of the obtained results lies very much on the correct estimation of the fracture energy as a material property. As for the softening law, better results are obtained using an exponential law, such as the one shown in Eq. (10) rather than linear softening law; the former providing longer tails in the post-critical response similar to the ones observed in experimental responses.

- As for the crack pattern it can be, at least when a reduced number of cracks are involved, precisely captured in both the onset and propagation aspects. In addition, mechanisms of sequential crack generation in the reinforcement neighborhood can be qualitatively reproduced. Whether or not this statement can be extended to more general crack patterns and stress states should be determined by subsequent works.

As for computational aspects, the CSDA exhibits the following features:

- The scheme is objective (mesh convergent) in terms of the mesh size and alignment, and fairly independent of the considered type of finite elements (triangular o quadrilateral).
- Even coarse finite element meshes provide acceptable solutions. This is a substantial advantage of using finite elements with embedded discontinuities. In contrast with alternative continuum methodologies, which require several (very small) finite elements to capture a displacement jump across their width, here that discontinuity is captured by only one element. This results in a reasonable computational cost and provides expectations on the viability of the CSDA for modeling cracking in larger concrete structures.

Acknowledgements

Financial support from the Spanish Ministry of Science and Technology, through grant MAT2001-3863-C03-03, and from the Catalan Government Research Department, trough the CIRIT grant 2001-SGR 00262, is gratefully acknowledged.

References

Armero, F. and Garikipati, K. (1996), "An analysis of strong discontinuities in multiplicative finite strain plasticity and their relation with the numerical simulation of strain localization in solids", *Int. J. Solids and Structures*, **33**, 20-22, 2863-2885.

Bazant, Z.P. (1986), "Mechanics of distributed cracking", *Appl. Mech. Review*, **39**(5), 675-702.

Borja, R.I. (2000), "A finite element model for strain localization analysis of strongly discontinuous fields based on standard Galerkin approximation", *Comput. Methods Appl. Mech. Eng.*, **190**, 1529-1549.

Cervera, M., Agelet de Saracibar, C. and Chiumenti, M. (2001), COMET: a multipurpose finite element code for numerical analysis in solid mechanics. Technical University of Catalonia (UPC).

Larsson, R., Runesson, K. and Sture, S. (1996), "Embedded localization band in undrained soil based on regularized strong discontinuity theory and finite element analysis", *Int. J. Solids and Structures*, **33**, 20-22, 3081-3101.

Lemaitre, J. (1985), "A continuous damage mechanics model for ductile fracture", *J. of Engineering Materials and Technology, Trans. ASME*, January 1985, **107**, 83-89.

Nechnech, W. (2000), "Contribution to the numerical analysis of concrete and reinforced concrete structures behaviour subjected to thermal and mechanical loads. A thermoelasto-plastic-damage approach", PHd Thesis, Lyon Applied Science National Institue, France. (In French). Available in : http://csidoc.insa-lyon.fr/these/2000/nechnech/.

Nooru-Mohamed, N.B. (1992), "Mixed mode fracture of concrete: an experimental approach", Ph.D. Thesis, Delft University of Technology, Delft, Netherlands.

NW-IALAD (2003), European Network "Integrity assessment of large dams", web page: http://nw-ialad.uibk.ac.at/Wp2/Tg2/Se2/Ss1.

Oliver, J. (1996), "Modeling strong discontinuities in solid mechanics via strain softening constitutive equations. Part1: Fundamentals; Part 2: Numerical simulation", *Int. J. for Numerical Methods in Engineering*, **39**, 3575-3623.

Oliver, J., Cervera, M. and Manzoli, O. (1999), "Strong discontinuities and continuum plasticity models: the strong discontinuity approach", *Int. J. of Plasticity*, **15**, 319-351.

Oliver, J. (2000), "On the discrete constitutive models induced by strong discontinuity kinematics and continuum constitutive equations", *Int. J. Solids and Structures*, **37**, 7207-7229.

Oliver, J., Huespe, A.E., Pulido, M.D.G. and Chaves, E. (2001), "From continuum mechanics to fracture mechanics: the strong discontinuity approach", *Engineering Fracture Mechanics*, **69**(2), 113-136.

Oliver, J., Huespe, A.E., Samaniego, E. and Chaves, E.W.V. (2002), "On strategies for tracking strong discontinuities in computational failure mechanics, proceedings of the fifth world congress on computational mechanics (WCCM V)", Editors: Mang, H.A.; Rammerstorfer, F.G.; Eberhardsteiner, J., Publisher: Vienna University of Technology, Austria, ISBN 3-9501554-0-6, http://wccm.tuwien.ac.at

Oliver, J., Huespe, A.E. and Samaniego, E. (2003a), A Study of finite elements for capturing strong discontinuities. *Int. J. for Numerical Methods in Engineering*, **56**, 2135-2161.

Oliver, J. and Huespe, A.E. (2003b), "Theoretical and computational issues in modeling material failure in Strong discontinuity scenarios", Accepted *Comp. Meth. Appl. Mech. Eng.*

Rots, J.G. (1988), "Computational modeling of concrete fracture", PhD Thes, Delft University of Technology.

Runesson, K, Ottosen, N.S. and Peric, D. (1991), "Discontinuous bifurcations of Elastic-plastic Solutions at Plane Stress and Plane Strain", *Int. J. Plasticity*, **7**, 99-121.

Simó, J.C., Oliver, J. and Armero, F. (1993), "An analysis of strong discontinuities induced by strain-softening in rate-independent inelastic Solids", *Computational Mechanics*, **12**, 277-296.

Spencer, B. (2002), "Finite elements with embedded discontinuity for modeling reinforced concrete members", Ph.D. Thesis, Dept. Civil, Env. Arch. Eng., University of Colorado. Colorado, U.S.A.

Wells, G.N. and Sluys, L.J. (2000), "Application of embedded discontinuities for softening Solids", *Engineering Fracture Mechanics*, **65**, 263-281.